PERGAMON

Solid State Communications 121 (2002) 447–452

solid state communications

www.elsevier.com/locate/ssc

High pressure behaviour of TbN: an X-ray diffraction and computational study

J.M. Jakobsen[a], G.K.H. Madsen[b], J.-E. Jørgensen[a,*], J. Staun Olsen[c], L. Gerward[d]

[a]*Department of Chemistry, University of Århus, DK-8000 Århus C, Denmark*
[b]*Institute for Physical and Theoretical Chemistry, TU Vienna, A-1060 Vienna, Austria*
[c]*Oersted Laboratory, Niels Bohr Institute, University of Copenhagen, DK-2100 Copenhagen, Denmark*
[d]*Department of Physics, Technical University of Denmark, DK-2800 Kgs. Lyngby, Denmark*

Received 26 March 2001; received in revised form 1 August 2001; accepted 8 August 2001 by J. Kuhl

Abstract

In the present work, we report an X-ray powder diffraction study of TbN up to an applied hydrostatic pressure of 43 GPa. TbN was found to be stable in the B1 (NaCl structure) within the examined pressure interval, and the zero pressure bulk modulus was determined to be 176(7) GPa. The electronic structure of ferromagnetic TbN has been studied using the linearized augmented plane-wave method. The calculated equilibrium volume and equation of state (EOS) for TbN agree poorly with experiment when the LDA and GGA versions of DFT were used. The agreement between the experimental and theoretical EOS is greatly improved by introducing an orbital dependent U term into the energy-functional. The 4f electrons in TbN-B1 are atomic like and highly correlated, and ferro-magnetic TbN-B1 is found to be a magnetic half-metal. Calculations find the spin-down f-electrons in a hypothetical TbN-B2 (CsCl) structure to be itinerant and well described by standard DFT functionals. No pressure-induced phase transitions were found below 250 GPa with the LDA + U and GGA + U methods.

PACS: 81.40.V; 61.10; 721.20

Keywords: High pressure; C. X-ray scattering; D. Electronic band structure

1. Introduction

The properties of the rare earth containing solids depend on the nature of, and interaction between, the 4f-electrons and the 6s and 5d electrons. The chemical bonding is mainly determined by the 6s and 5d electrons and the magnetism by the localized atomic-like 4f-electrons [1]. The delicate balance between the 4f-shell and the 6s and 5d electrons varies with interatomic distance and can be perturbed by externally applied pressure. Several pressure-induced valence and structural phase transitions have been found experimentally in the rare earth chalcogenides[1] and pnictides [12–18].

Structural phase transitions from the NaCl (B1) to the CsCl (B2) structure have been observed for EuX, for X = O, S, Se and Te at elevated pressure [5–11]. The transition pressures for these compounds are 39.0, 21.0, 14.5 and 11.0 GPa, respectively. Similar phase transitions have also been observed in YbX for X = S, Se and Te as well as in the case of SmX for X = Se and Te [5–11]. In addition to the structural B1 to B2 transitions, rare earth valence changes have been observed in several of the rare earth chalcogenides. YbSe and YbS exhibit anomalous compression curves in the pressure range 15–20 GPa which are considered to be due to a change in the Yb valency and optical reflectivity measurements have also shown the onset of a 4f-shell instability near 10 GPa [9]. Evidence for a valence transition around 12.5 GPa has also been found in CeS [2]. Furthermore, in addition to the structural B1 to B2 transition, it has been shown that EuO exhibits an isostructural phase transition indicating a valence change at 30 GPa resulting in a 4% reduction of the volume. However, later

* Corresponding author. Tel.: +45-8942-3333; fax: +45-8619-6199.

E-mail address: jenserik@kemi.aau.dk (J.-E. Jørgensen).

[1] For cerium chalcogenides see Refs. [2–4]. For Pr, Nd, Sm, Gd, Tb, Eu and Yb chalcogenides see Refs. [5–11].

0038-1098/02/$ - see front matter
PII: S0038-1098(01)00506-3

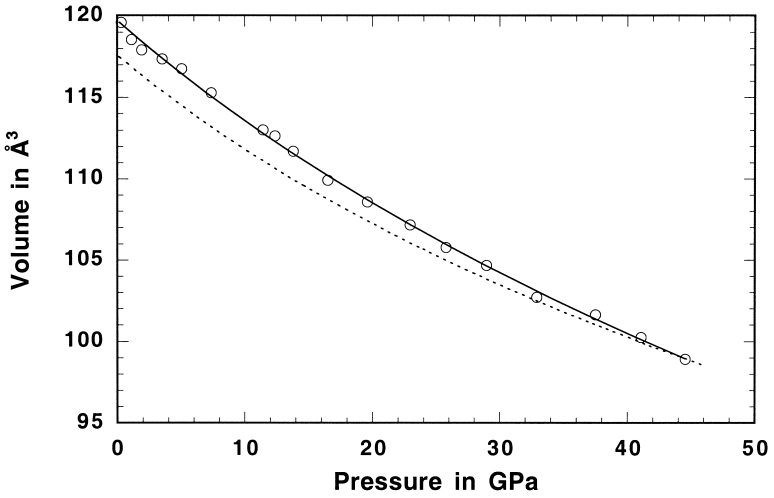

Fig. 1. Volume versus pressure for TbN. The solid line represents a fit of the Birch type EOS with $B_0 = 176(7)$ GPa and $B_0' = 3.1(3)$. The dotted line corresponds to the LDA + $U6$ model in Table 1.

work just confirmed the B1 to B2 transition which was observed to start at 47 GPa [10] but peculiarities in the magnetic order of EuO were observed above 10 GPa [11]. Among the rare earth pnictides CeP exhibits an electronic transition associated with a volume change of 8% at about 10 GPa [12]. The transition is isostructural and it is due to a change in the valence state of Ce, which changes from +3 to +4. A similar transition was expected for CeAs, but only a structural B1 to B2 transition around 15 GPa has been observed experimentally [13,14]. CeSb exhibits a structural transition at 11 GPa during which the crystal structure changes from the B1 structure to a tetragonally distorted B2 structure, and no change of the Ce valency was observed up to 25 GPa [15].

Cerium, praseodymium and terbium are known to exist in both oxidation states three and four in chemical compounds. Compounds containing one of these rare earth ions in the trivalent form are therefore candidates for pressure-induced phase transitions. Rare earth nitrides crystallize in the NaCl structure at ambient pressure and the rare earth ions are considered to be in oxidation state three. However, the rare earth nitrides and nitrides in general are much less studied than the corresponding chalcogenides and heavier pnictides due to the fact that they in most cases are more difficult to prepare and less stable. We have therefore undertaken a study of the high-pressure behaviour of rare earth nitrides, and in the present work we report a high-pressure X-ray powder diffraction study of TbN. Furthermore, we report a computational study of the electronic structure of TbN in the B1 and B2 structures and compare the calculated equilibrium unit cell volumes and equation of state (EOS) data with the corresponding measured quantities.

2. Experimental procedure

TbN was synthesized by direct nitration of Tb as described by Kieffer et al. [19]. A Tb lump was heated in a radio frequency induction furnace in an N_2 atmosphere. Several heating steps were performed and the sample was investigated in between to check the degree of conversion. The duration of each step was up to 7 h, and the maximum heating temperature was 1300 °C under a maximum N_2 pressure of 500 kPa.

X-ray powder diffraction patterns were recorded with synchrotron radiation using the white-beam energy-dispersive method. High-pressure conditions were obtained in a Syassen–Holzapfel type diamond anvil cell. The sample and a small ruby chip were enclosed in a hole of diameter 0.2 mm in an Inconel gasket. For the pressure-transmitting medium, we used silicone oil. No difference in data recorded with the two pressure-transmitting media was found. The actual pressure was determined by the ruby fluorescence method. The uncertainty in the pressure determination is estimated to be 0.1 GPa for pressures below 15 GPa. For higher pressures, the uncertainty may be larger because of possible non-hydrostatic conditions. The Bragg angle associated with each experimental run was determined from a zero-pressure diffraction pattern of NaCl.

3. Computational procedure

The linearized augmented plane wave (LAPW) method as embodied in the WIEN97 code [20], has been employed. The density functional theory (DFT) exchange and correlation potentials were calculated both in the local spin

Table 1
Calculated and experimental equilibrium lattice constants and bulk moduli for TbN in the B1 structure. The LDA + U and GGA + U calculations are marked with a number which corresponds to the onsite correlation term U (eV) used in the specific calculation

	Primitive vol. (a.u.)	a_0 (Å)	B_0 (GPa)	B_0'
Experimental	202.521	4.933	176(7)	3.1(3)
LDA	183.267	4.771	180.6	4.9
GGA	198.636	4.901	139.9	4.4
LDA + $U4$	197.645	4.893	187.4	4.5
LDA + $U6$	198.352	4.899	179.2	4.2
GGA + $U4$	208.910	4.984	154.5	4.2
GGA + $U6$	206.302	4.964	154.2	3.9

density approximation and with the generalized gradient approximation in the form reported by Perdew et al. [21]. For some of the calculations, an orbital dependent potential is introduced for the f-electrons through a Hubbard U [22–24]. In all LDA + U calculations, the Stoner J was set to $U/8$. To improve the linearization, the augmented plane wave basis set was extended with local orbitals [25] for the terbium 5s and 5p and the nitrogen 2s states. The Rk_{max} was 7 for all calculations and the irreducible Brillouin zone (IBZ) was sampled at 104 k-points in the B1 structure and at 120 k-points in the B2 structure. All calculations were carried out with a ferro-magnetic ordering of the spins [26].

4. Experimental results

Powder patterns of TbN were recorded in the pressure range 0–43 GPa and all reflections in the measured patterns were indexed on fcc unit cells showing that no structural B1 to B2 transition is taking place within the measured pressure range. Fig. 1 shows the volume versus pressure curve for TbN, and the solid line represents a fit to the Birch-type EOS [27]

$$P = \tfrac{3}{2}B_0(x^{-7/3} - x^{-5/3})[1 - \tfrac{3}{4}(4 - B_0')(x^{-2/3} - 1)], \qquad (1)$$

where x denotes the volume ratio V/V_0 with V_0 being the volume at zero pressure while B_0 and B'_0 are the isothermal bulk modulus at ambient pressure and its pressure

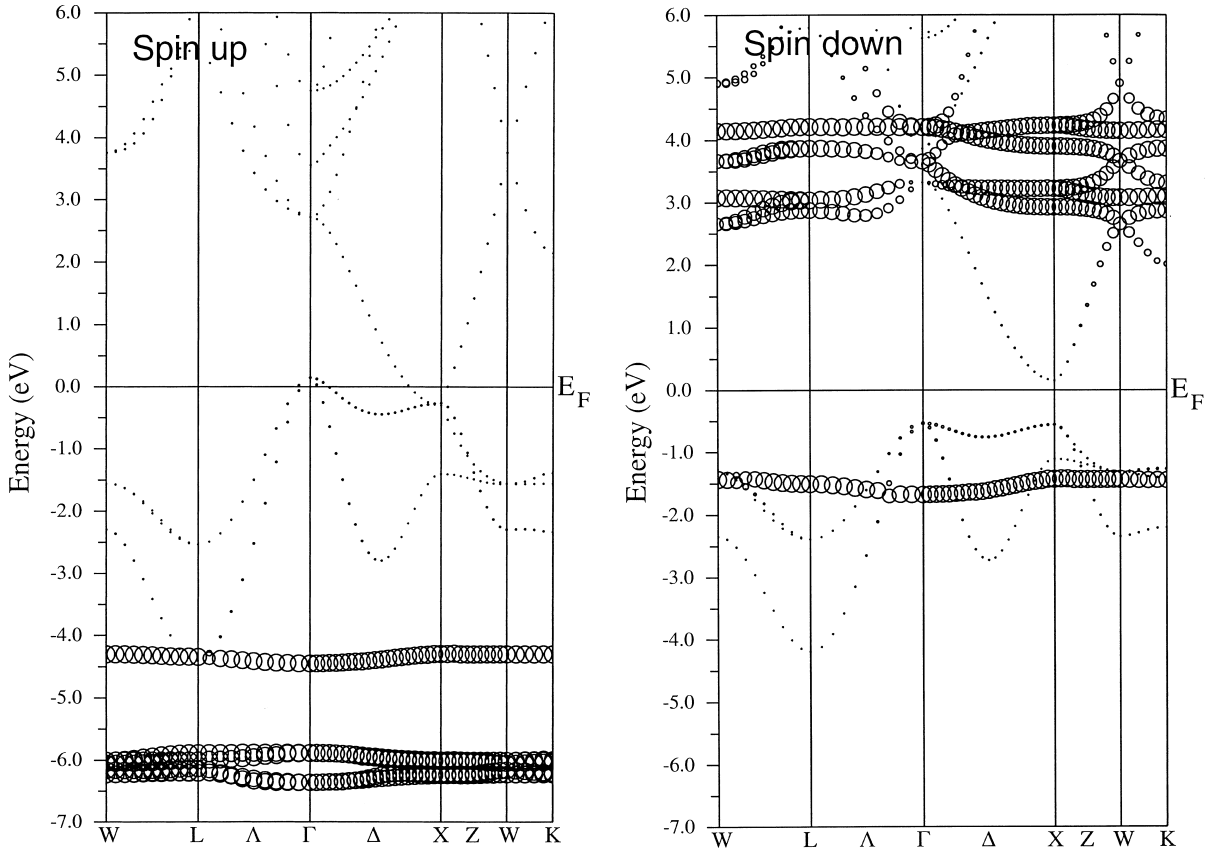

Fig. 2. Band structure of the spin-up and spin-down electrons for TbN in the B1 structure. The size of the circles is proportional to the f-character of the state. The symbols label special points within the first Brillouin zone. W: $k = (2\pi/a)(1, 1/2, 0)$, L: $k = (2\pi/a)(1/2, 1/2, 1/2)$, Γ: $k = (0, 0, 0)$, X: $k = (2\pi/a)(1, 0, 0)$, K: $k = (2\pi/a)(3/4, 3/4, 0)$.

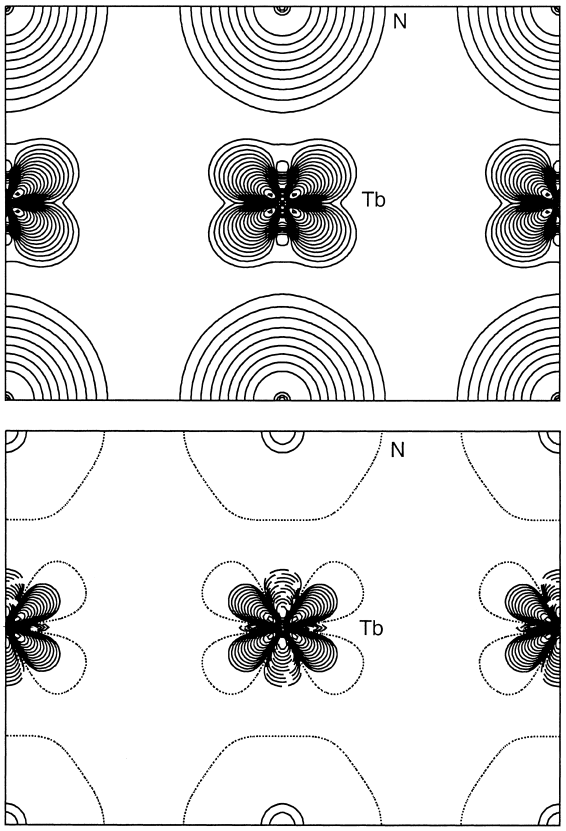

Fig. 3. Spin-down valence electron density (eigen-energies down to 6 eV below the Fermi energy) in the [110] plane of TbN in the B1 structure. Contour values are $0.01 \times 2^{n/2}$ e a.u.$^{-3}$. The dotted line is the zero contour. The broken lines are the negative contours and the full lines the positive. (a) Calculated with the LDA approximation including a U term of 6 eV. The maximum along (111) direction is 2.00 e a.u.$^{-3}$. (b) Difference valence density between the LDA + U6 density and the pure LDA calculation. The maximum along (111) direction is 0.09 e a.u.$^{-3}$.

derivative, respectively. The fact that the p–V behaviour can be described by the Birch-type EOS shows that no isostructural phase transition, indicating a valence transition of Tb is taking place within the investigated pressure range. The least squares fit to the measured data yields the following values for the bulk modulus and its pressure derivative: $B_0 = 176(7)$ GPa and $B_0' = 3.1(3)$.

No measured bulk moduli for the rare earth nitrides are to the best of our knowledge available in the literature. However, a calculated bulk modulus of 159 GPa for CeN has recently been determined by Svane et al. [28]. This value is in good agreement with the value of 153 GPa determined from preliminary X-ray diffraction data [29]. Comparable values have been determined for the 5f nitrides UN ($B_0 = 203(3)$ GPa and $B_0' = 6.3(6)$) and ThN ($B_0 = 175(15)$ GPa and $B_0' = 4.0(4)$) [30].

5. Computation results

5.1. TbN in the B1 structure

Total energies were calculated as a function of unit cell volume. Bulk moduli and equilibrium volumes were determined from the fitted EOS. The results are given in Table 1. As can be seen, the LDA calculations significantly underestimate the equilibrium unit cell volume. The GGA calculations give a unit cell volume in good agreement with experiment. However, the bulk modulus is predicted significantly smaller than the experimentally observed. It is well known that strong onsite correlations between the f-electrons in several rare-earth compounds are poorly described in standard DFT methods [1]. One successful approach for f-electron systems has been the SIC-LDA [1,28,31]. Another approach has been the so-called LDA + U energy functional where the atomic like orbitals are singled out and a Hubbard type U is included in the DFT total energy functional [22]. Table 1 shows that the introduction of U in the LDA calculation leads to a significant improvement in the calculated unit cell volume. Also the calculated bulk modulus is in good agreement with the experimentally observed. The p–V curve calculated according to the LDA + U6 model are also shown in Fig. 1 for comparison with the corresponding experimentally determined curve. The LDA + U6 model is seen to underestimate the volume while the calculated bulk modulus is in good agreement with the experimentally determined value. The GGA + U calculations overestimate the unit cell volume and underestimate the bulk modulus and are thus in poorer agreement with experiment than the LDA + U calculations.

In the LDA and GGA the spin moment is found to be $6\mu_B$ per Tb atom as expected. However, there is not simply one filled f-band. The spin down f-bands cross each other and are found in a relatively broad (compared to the spin up f-electrons) energy range at the Fermi level. This situation is changed by the introduction of the U. This leads to a splitting of the spin down bands of a magnitude similar to the introduced U, Fig. 2, which transforms TbN-B1 into a magnetic half-metal. The spin-down f-electrons now occupy a single narrow f-state. While the actual splitting and position of the f-bands depend on the magnitude of the U, the calculated EOS is less affected. This means that the change in chemical bonding is relatively independent of the magnitude of the introduced U. Fig. 3(a) and (b) shows that, compared to the pure LDA calculation, the LDA + U calculation strengthens a polarization of the f-electrons that was already there in the LDA calculation. Furthermore the spin-down f-like electrons are concentrated closer to the TbN nucleus. These two effects are the direct-space equivalents of, respectively, the lowering and change hybridization of the spin-down f-bands.

5.2. Pressure-induced phase transition

As mentioned in Section 1 B1 to B2 pressure-induced

Table 2
Calculated equilibrium lattice constants and bulk moduli for TbN in the B2 structure. The LDA + U and GGA + U calculations are marked with a number which corresponds to the onsite correlation term U (eV) used in the specific calculation

	Primitive vol. (a.u.)	B_0 (GPa)	B_0'
LDA	165.474	174.6	4.7
GGA	179.847	136.6	4.6
LDA + $U4$	165.174	179.8	5.1
LDA + $U6$	165.226	179.2	5.1
GGA + $U4$	179.880	136.3	4.6
GGA + $U6$	179.909	136.3	4.6

structural phase transitions have been observed for all cerium–pnictides except CeN [2–4,28]. As no experimental phase transition was observed in TbN in the examined pressure range, the possibility for a B1 to B2 transition in the case of TbN has been investigated computationally. Equilibrium volumes and bulk moduli for the hypothetical TbN-B2 structure are given in Table 2. The B1 and B2 structures have very similar equilibrium primitive unit cell volumes and bulk moduli, but the B2 structure is found to be significantly higher in energy, meaning that a very high critical pressure for the phase transition must be expected. As opposed to the situation in the B1 structure, the introduction of U only changes the calculated EOS slightly. Band structure plots also show that a high density of states of spin down electrons of f-character is found at the Fermi level, in all calculations. The spin down f-electrons are therefore predicted to be itinerant and to contribute to metallic conductivity. Valence density plots similar to Fig. 3(a) also showed that the spin down f-electrons in TbN-B2 are distributed almost spherically around the Tb positions, confirming that the f-electrons in TbN-B2 are itinerant rather than atomic-like.

From the EOS, the free energy as a function of pressure can be calculated. No pressure-induced phase transition is found below 250 GPa in the calculations that include a U in the energy functional. With the pure LDA and GGA calculations, critical pressures for the phase transition are calculated to 107.5 and 132 GPa, respectively. However, in view of the poor agreement between the calculated and measured EOS in the B1 structure with LDA and GGA, these values are probably unreliable.

6. Conclusion

The pressure–volume curve measured up to a pressure of 43 GPa in the high pressure X-ray diffraction experiment is well described by the Birch EOS. TbN is therefore stable in the B1 structure, and no valence change of Tb takes place in the investigated pressure range. The agreement between the experimental and theoretical EOS was greatly improved by introducing the orbital dependent U term into the energy-functional. The effect of the Hubbard U is both to split the spin down f-states at the Fermi level and to increase the polarization of the spin down f-electrons. No pressure-induced phase transitions are found below 250 GPa with the EOS calculated by the LDA + U and GGA + U methods.

Acknowledgements

We thank HASYLAB-DESY for permission to use the synchrotron radiation facility. Financial support from the Danish Natural Science Research Council and DANSYNC is gratefully acknowledged. The project was supported by the IHP Programme 'Access to Research Infrastructures' of the European Commission (Contract HPRI-CT-1999-00040).

References

[1] P. Strange, A. Svane, W.M. Temmerman, Z. Szotek, H. Winter, Nature 399 (1999) 756.
[2] M. Croft, A. Jayarama, Solid State Commun. 35 (1980) 203.
[3] J.M. Leger, R. Epain, J. Loriers, D. Ravot, J. Rossat-Mignod, Phys. Rev. B 28 (1983) 7125.
[4] J.M. Leger, A.M. Redon, J. Less-Common Met. 156 (1989) 137.
[5] A. Chatterjee, A.K. Singh, A. Jayaramen, Phys. Rev. B 6 (1972) 2285.
[6] A. Jayaraman, A.K. Singh, A. Chatterjee, S. Usha Devi, Phys. Rev. B 9 (1974) 2513.
[7] K. Syassen, Physica B 139 (1986) 277.
[8] J. Hayashi, I. Shirotani, Y. Tanaka, T. Adachi, O. Shimomura, T. Kikegawa, Solid State Commun. 114 (2000) 561.
[9] K. Syassen, H. Winzen, H.G. Zimmer, H. Tups, J.M. Leger, Phys. Rev. B 32 (1985) 8246.
[10] S. Heathman, T. Le Bihan, S. Darracq, C. Abraham, D.J.A. De Ridder, U. Benedict, K. Mattenberger, O. Vogt, J. Alloys Compd 230 (1995) 89.
[11] I.N. Goncharenko, I. Mirebeau, A. Ochiai, Hyperfine Interact. 128 (2000) 225.
[12] A. Jayaraman, W. Lowe, L.D. Longinotti, Phys. Rev. Lett. 36 (1976) 366.
[13] A. Werner, H.D. Hochheimer, R.L. Meng, E. Bucher, Phys. Lett. 97A (1983) 207.
[14] J.M. Léger, D. Ravot, J. Rossat-Mignod, J. Phys. C: Solid State Phys. 17 (1984) 4935.
[15] J.M. Leger, K. Oki, J. Rossat-Mignod, O. Vogt, J. Phys. 46 (1985) 889.
[16] I. Vedel, A.M. Redon, J. Rossat-Mignod, O. Vogt, J.M. Leger, J. Phys. C 20 (1987) 3439.
[17] J.M. Leger, I. Vedel, A.M. Redon, J. Rossat-Mignod, J. Magn. Magn. Mater. 63 (1987) 49.
[18] N. Mori, Y. Okayama, H. Takahashi, Y. Haga, T. Suzuki, Physica B 186 (1993) 444.
[19] R. Kieffer, P. Ettmayer, Sw. Pajakoff, Monatsh. Chem. 103 (1972) 1285.
[20] P. Blaha, K. Schwarz, J. Luitz, WIEN97, a full potential linearized augmented plane wave package for calculating

crystal properties, ISBN 3-9501031-0-4, Tech. Universität Wien, Austria, 1999.
[21] J.P. Perdew, S. Burke, M. Ernzerhof, Phys. Rev. Lett. 77 (1996) 3865.
[22] V.I. Anisimov, J. Zaanen, O.K. Andersen, Phys. Rev. B 44 (1991) 943.
[23] A.B. Shick, A.I. Liechtenstein, W.E. Pickett, Phys. Rev. B 60 (1999) 10 763.
[24] P. Novak, P. Blaha, personal communication.
[25] D.J. Singh, Phys. Rev. B 43 (1991) 6388.
[26] W. Stutius, Physik Kondensierten Materie 10 152/85 (1969) 153.
[27] F. Birch, J. Appl. Phys. 9 (1938) 279.
[28] A. Svane, Z. Szotek, W.M. Temmerman, J. Lægsgaard, H. Winter, J. Phys. Condens. Matter 10 (1998) 5309.
[29] J.-E. Jørgensen, J. Staun Olsen, L. Gerward, unpublished.
[30] J. Staun Olsen, S. Steenstrup, L. Gerward, U. Benedict, J.-P. Itié, Physica B 139/140 (1986) 308.
[31] A. Svane, W.M. Temmerman, Z. Szotek, J. Lægsgård, H. Winter, Int. J. Quant. Chem. 77 (2000) 799.